

# History-Aware Transformation of ReID Features for Multiple Object Tracking

Ruopeng Gao<sup>1</sup>    Yuyao Wang<sup>1</sup>  
<sup>1</sup>Nanjing University

Chunxu Liu<sup>1</sup>    Limin Wang<sup>1,2, ✉</sup>  
<sup>2</sup>Shanghai AI Lab

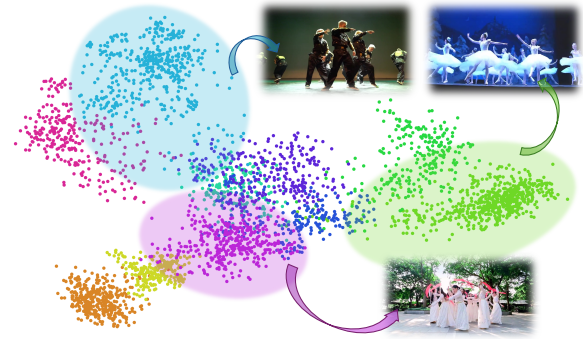
{ruopenggao, wayfareryy}@gmail.com, chunxu.liu@smail.nju.edu.cn, lmwang@nju.edu.cn

## Abstract

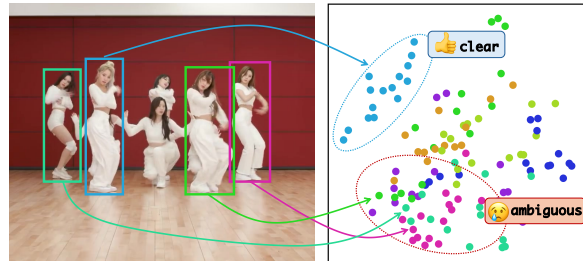
The aim of multiple object tracking (MOT) is to detect all objects in a video and bind them into multiple trajectories. Generally, this process is carried out in two steps: detecting objects and associating them across frames based on various cues and metrics. Many studies and applications adopt object appearance, also known as re-identification (ReID) features, for target matching through straightforward similarity calculation. However, we argue that this practice is overly naive and thus overlooks the unique characteristics of MOT tasks. Unlike regular re-identification tasks that strive to distinguish all potential targets in a general representation, multi-object tracking typically immerses itself in differentiating similar targets within the same video sequence. Therefore, we believe that seeking a more suitable feature representation space based on the different sample distributions of each sequence will enhance tracking performance. In this paper, we propose using history-aware transformations on ReID features to achieve more discriminative appearance representations. Specifically, we treat historical trajectory features as conditions and employ a tailored Fisher Linear Discriminant (FLD) to find a spatial projection matrix that maximizes the differentiation between different trajectories. Our extensive experiments reveal that this training-free projection can significantly boost feature-only trackers to achieve competitive, even superior tracking performance compared to state-of-the-art methods while also demonstrating impressive zero-shot transfer capabilities. This demonstrates the effectiveness of our proposal and further encourages future investigation into the importance and customization of ReID models in multiple object tracking. The code will be released at <https://github.com/HELLORPG/HATReID-MOT>.

## 1. Introduction

Multiple object tracking (MOT) is a longstanding and continually evolving task in computer vision, with the goal of detecting all objects in a video and associating objects of the same identity across different frames to form continu-



(a) Visualizing different sequences in DanceTrack [40]. It illustrates that each sequence’s ReID features only occupy a limited area within the original space.



(b) Displaying the ReID features of different trajectories in the sequence. Due to their high similarity, some identities cannot be well distinguished in the original space.

Figure 1. Visualization of re-identification features in the original representation space [24].

ous trajectories. As a fundamental task, multi-object tracking serves as a middleware for various downstream research and applications, such as trajectory prediction, action analysis, autonomous driving, security surveillance, and so on.

Over the course of its development, the tracking-by-detection paradigm has gradually become dominant. These approaches [3, 49] divide the problem into two subtasks: detection and association, with the latter becoming the primary focus of intense research efforts. Within this context, various information modalities [1, 3, 9, 35] are utilized in

✉: Corresponding Author

the matching strategy, while object appearance is an essential member of them. With the help of large-scale training data, feature extractors [24, 41] can produce reliable representations to distinguish the appearance characteristics of different trajectories, optimizing match selections in multi-object tracking.

Although the introduction of appearance features [27, 42, 48] has led to notable success, we still observe some disharmony. In the MOT community, most methods [26, 41] follow the standard re-identification (ReID) task when incorporating feature information, independently calculating the similarity of ReID features at each moment. However, we argue that the pursuits of these two tasks during inference are not entirely aligned. For re-identification tasks, the objective is to distinguish all potential targets as much as possible, leaning towards more general needs. As for multi-object tracking, its goal is to focus on differentiating similar objects within the current sequence, which is more inclined towards expert demands. We point out that this leads to significant differences in their requirements for target representation, making the direct use of the original ReID feature space inefficient and inaccurate. On the one hand, in the same video, target features usually take up only a subset of the original space due to the limited identities, making the rest of the representation space redundant, as shown in Fig. 1a. On the other hand, targets within the same sequence may be extremely similar, and such minor differences are hard to clearly represent in the general space, causing ambiguity and confusion, as illustrated in Fig. 1b. Based on the above analysis, we believe that for each video sequence during inference, a more specialized representation is needed to boost tracking performance.

In this paper, we treat historical target features as conditions and apply Fisher Linear Discriminant (FLD) [11] to find a projection matrix. According to the definition, this allows us to find a representation space that maximizes inter-trajectory differences and minimizes intra-trajectory differences, perfectly fitting the pursuit of distinguishing similar targets within a single sequence. Since Fisher Linear Discriminant has a close-form analytical solution, we can directly use it upon the extracted ReID features without additional training or modifying other components. Our experimental results have shown that this straightforward approach can substantially enhance the discriminative capacity of ReID features, thus promoting better tracking performance. Nevertheless, we have revisited this methodology and introduced several custom modifications tailored for the tracking task. Firstly, the feature center of each trajectory is vital as it determines the distribution center of each trajectory after projection. Different from conventional classification tasks, the ReID features in online tracking are constantly changing, and usually, only the features closest to the current frame are the most similar. Therefore, we sug-

gest that temporal information should be considered when calculating the feature center, rather than relying on a naïve averaging across all time steps. Practically, we employ a dynamic weight coefficient to move the trajectory centroid closer to the current features, called *Temporal-Shifted Trajectory Centroid*. Secondly, although using only the projected features can yield significant performance improvements, we should not disregard the importance of the original feature space. We suggest that the specialization and generation of those two representation spaces can complement each other. Hence, we perform a weighted sum of the similarity results from both spaces to construct a *Knowledge Integration*.

Our extensive experiments on multiple benchmarks demonstrate that the aforementioned method can significantly improve the performance of feature-based trackers, making them comparable to or better than state-of-the-art methods. The incremental and comprehensive ablation studies have validated the effectiveness of each component. Furthermore, as our method only relies on historical trajectories without the need of training samples, we also explore its effectiveness in zero-shot multi-object tracking and observe notable improvements. Finally, this paper not only brings obvious tracking performance enhancement but also seeks to inspire the reconsideration of using appearance features in MOT tasks. Through discussing and validating the divergences between MOT and regular ReID tasks, we aspire to encourage the creation of more specialized feature extraction and matching techniques tailored for MOT, thus increasing the dependability and practicality of target features for object association.

## 2. Related Work

**Tracking-by-Detection** is the most widely used paradigm for multiple object tracking. According to the definition, MOT is divided into two separate sub-tasks: detection and association. Although there are a few approaches [17] investigating custom detectors, the majority of studies [10, 16, 21, 22, 28, 37, 51, 52] concentrate on different association strategies. Typically, the Kalman filter is employed to provide linear estimations of target movement, thus predicting their current positions and matching them with detected objects [3, 45]. ByteTrack [49] proposed a multi-stage cascaded matching strategy that allows low-confidence bounding boxes to be correctly associated. With the introduction of more intricate tracking scenarios, numerous approaches [5, 10, 46] incorporated tailored algorithms to handle non-linear and abrupt motion patterns, while some other studies [9, 16, 26, 33, 43] seek learnable estimation modules to address the diversity of motion. Unlike the diverse development of motion information, although some research [41, 48] has explored joint detection and embedding in a unified model, appearance cues

are often simply inserted as an additional option in motion-based algorithms [26, 27, 42, 46]. We believe this is because the discriminative capability of the ReID features are not enough to challenge the dominance and priority of motion information. By focusing on increasing the separation ability of existing ReID features, we seek to reclaim their place in the spotlight. Moreover, many works [1, 9] have attempted to use more modalities in matching algorithms to develop more comprehensive association strategies.

**End-to-End MOT** is an emerging force, bypassing manual heuristic algorithms in favor of formulating multi-object tracking in an end-to-end manner [14, 47]. A typical form is to expand DETR [6, 53] into MOT tasks, representing different trajectories through the propagation of track queries [29, 39, 47]. Follow-up methods incorporated temporal information [4, 13, 38] and mitigated the imbalance of supervision signals [44, 50], leading to better tracking performance. Nevertheless, end-to-end methods still face the challenges of high computational costs and a strong need for training data, requiring future research to tackle.

### 3. Method

#### 3.1. Preliminary

For typical tracking-by-detection trackers, each frame is processed in two steps. Firstly, given the current input frame  $I_t$ , the detector  $\mathcal{D}$  produces all bounding boxes  $B_t = \{b_1^t, \dots, b_i^t, \dots\}$  for the objects of interest. Secondly, a range of information and hand-crafted algorithms are applied to associate all detection results  $B_t$  with historical trajectories  $\mathcal{T} = \{\tau_1, \tau_2, \dots, \tau_{N_{id}}\}$  or to mark them as new-born targets. Although there are various association cues (shown in Sec. 2), as discussed in Sec. 1, our focus is on the association branch based on ReID features. Generally, an additional feature extraction network (or called ReID model)  $\Theta$  is used to extract the ReID feature of a given bounding box, as formulated below:

$$\mathbf{f}_i^t = \Theta(I^t, b_i^t), \quad (1)$$

where  $\mathbf{f}_i^t$  denotes the ReID feature corresponding to the detection result  $b_i^t$ . Likewise, for every trajectory  $\tau_j$ , we must keep an updated trajectory feature  $\hat{\mathbf{f}}_j$ . This feature is continuously refined through online inference (typically by Exponential Moving Average), ensuring it appropriately represents the trajectory.

In the matching process for each frame, target features are assumed to be linearly separable. Consequently, cosine similarity is widely used to measure the similarity between detection results and trajectories:

$$\cos(\mathbf{f}_i^t, \hat{\mathbf{f}}_j) = \frac{\mathbf{f}_i^t \cdot \hat{\mathbf{f}}_j}{\|\mathbf{f}_i^t\| \|\hat{\mathbf{f}}_j\|}, \quad (2)$$

where  $\mathbf{f}_i^t$  indicates the ReID feature of the  $i$ -th detection in the current frame  $I^t$ , while  $\hat{\mathbf{f}}_j$  represents the online feature of the  $j$ -th trajectory. Afterward, these similarity values are used to calculate the cost matrix, serving as input for heuristic algorithms to determine the final association results.

It is worth noting that there are numerous customized variants [1, 32, 42] of the ReID branch. For simplicity, we primarily focus on the most widely used form today [1, 26, 27]: updating trajectory features through naïve EMA for each frame, using  $-\cos(\mathbf{f}_i^t, \hat{\mathbf{f}}_j)$  for the cost matrix, and employing the Hungarian algorithm for optimal assignment.

#### 3.2. History-Aware Projection of ReID Features

Usually, the target feature extractor  $\Theta$  is exposed to a large and diverse collection of samples during the training stage, acquiring general and robust representations through contrastive learning [24, 32]. However, as discussed in Sec. 1, this representation space might be suboptimal for multiple object tracking. On the one hand, in a continuous video sequence, the distribution of object features might be limited to a small area of the original space, as shown in Fig. 1a, resulting in inefficient and redundant use of the representations. On the other hand, the objects that need to be tracked within the same video might be extremely similar, and such slight differences are difficult to distinguish in general representations, as illustrated in Fig. 1b, which results in confusion during target association. Therefore, we suggest finding a more specialized feature space for each sequence during inference, in order to enhance the discriminative capability for similar targets and reduce ambiguity.

Motivated by the aforementioned, we naturally arrive at an implementation that employs Fisher Linear Discriminant (FLD) [11] for the linear projection of the feature space. To start, we review the definition of Fisher Linear Discriminant. Given a set of  $N$  feature vectors  $\{x_1, x_2, \dots, x_N\} = X \in \mathbb{R}^{N \times D}$ , each feature  $x$  is associated with one of  $C$  classes. The objective of FLD is to find a projection matrix  $W \in \mathbb{R}^{D \times D'}$  that maximizes the distance between the class means after projection while minimizing the within-class covariance. This will provide a subspace with better separation capabilities [11, 34]. To express it mathematically, denote  $X_c$  as the subset of  $X$  pertaining to class  $c$ , where  $N_c$  and  $m_c$  represent the size and mean of  $X_c$ , respectively. Then FLD calculates within-class scatter matrix  $S_W$  and between-class scatter matrix  $S_B$  as:

$$S_W = \sum_{c=1}^C \sum_{x \in X_c} (x - m_c)(x - m_c)^T, \quad (3)$$

$$S_B = \sum_{c=1}^C N_c (m_c - m)(m_c - m)^T, \quad (4)$$

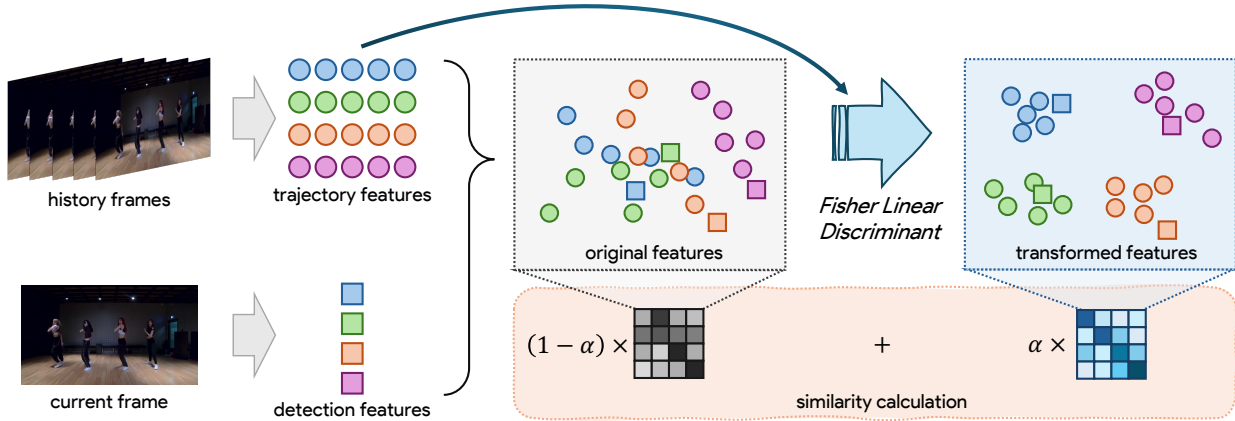


Figure 2. **Overview of our pipeline.** We use different colors to indicate different identities (trajectories). In the original space, some overly similar targets cannot be well distinguished, leading to issues in the current frame’s matching process. Therefore, we treat the trajectory features as conditions and apply a modified *Fisher Linear Discriminant* to seek a more optimal space for distinguishing different trajectories. Finally, both original and transformed features are used to calculate the similarity matrix, balancing generalization and specialization.

$$\mathbf{m} = \frac{1}{N} \sum_{i=1}^N \mathbf{x}_i, \quad (5)$$

$$\mathbf{m}_c = \frac{1}{N} \sum_{\mathbf{x} \in X_c} \mathbf{x}. \quad (6)$$

The Fisher criterion for multi-class problem is formulated as follow [12]:

$$\arg \max_W J(W) = \text{tr}\{(W^T S_W W)^{-1} (W^T S_B W)\}. \quad (7)$$

According to [12], the desired projection matrix  $W$  is composed of the eigenvectors of  $S_W^{-1} S_B$  corresponding to the largest  $D'$  eigenvalues, where  $D' = \min(C - 1, D)$ .

During the tracking process for each sequence, we treat each trajectory as a class, and each ReID feature  $\mathbf{f}$  as a feature vector  $\mathbf{x}$ . This forms the corresponding derivations of Eq. (4, 3, 5, 6) in the MOT context. In this way, through the processing of Fisher Linear Discriminant, we can acquire a projection matrix  $W$  to maximize the distinctions between different trajectories, thus enhancing the discriminative ability for similar targets. The transformed ReID feature can be expressed as  $\mathbf{f}' = \mathbf{f}W$ , and will be used to calculate the similarity according to Eq. (2).

### 3.3. Temporal-Shifted Trajectory Centroid

As described in 3.2, we calculate the mean of ReID features for each trajectory. In practice, since the inference sequence can be temporally unbounded, we limit our consideration within the most recent  $T$  frames. For each trajectory  $\tau_j$ , we manage a first-in-first-out feature queue  $\mathcal{F}_j =$

$\{\mathbf{f}_j^{t-1}, \mathbf{f}_j^{t-2}, \dots, \mathbf{f}_j^{t-T}\}$ , and all of these feature queues  $\mathcal{F} = \{\mathcal{F}_1, \mathcal{F}_2, \dots, \mathcal{F}_{N_{id}}\}$  are used for the calculations in Eq. (3 - 6). Hence, the calculation of the trajectory centroid at time step  $t$  can be written as:

$$\mathbf{f}_j = \frac{1}{T} \sum_{t'=1}^T \mathbf{f}_j^{t-t'}, \quad (8)$$

where  $\mathbf{f}_j^{t-t'}$  indicates the ReID feature of the  $j$ -th trajectory at time step  $t - t'$ . Although our experimental results verify that such a naïve averaging can lead to substantial improvements, we still need to highlight that it neglects the temporal information in MOT tasks.

Different from traditional classification tasks, in online tracking, targets could experience deformation and occlusion, causing the object features to change constantly. As a result, even within the same trajectory, the similarity of targets may decrease as the time interval increases. This observation indicates that ReID features closer to the current frame are more critical and reliable for target association. According to the definition [11], the sample center in Eq. (4) determines the center of the distribution after projection. Thus, we propose shifting it toward the current moment to better accommodate the requirements of online tracking. Specifically, we use a dynamic weight  $\lambda_{t'}$  to adjust the centroid calculation, as follows:

$$\mathbf{f}_j = \frac{1}{\sum \lambda_{t'}} \sum_{t'=1}^T \lambda_{t'} \mathbf{f}_j^{t-t'}, \lambda_{t'} = (\lambda_0)^{t'}. \quad (9)$$

We set  $0.0 < \lambda_0 < 1.0$ , giving larger weight to ReID features closer to the current time step  $t$  to achieve a temporal

shift of the trajectory centroid. The same implementation will also be applied to the calculation in Eq. (5).

### 3.4. Knowledge Integration

Applying the approach from Sec. 3.2 and Sec. 3.3, we can obtain the required projection matrix  $W$  by solving the eigenvectors then calculate the similarity  $\cos(\mathbf{f}_i^{t'}, \hat{\mathbf{f}}_j')$  in the corresponding subspace. While this has resulted in significant improvements in tracking performance, as shown in Tab. 5, we still need to emphasize that this does not imply that the original representation space is without merit. On the one hand, there are potential risks in calculating the projection matrix based on previously tracked targets, as it may become unreliable when faced with ID misallocation. On the other hand, untransformed features exhibit stronger generalization capabilities, making them better for handling unseen targets. Therefore, we propose integrating the knowledge from these two different spaces, allowing their specialization and generalization capabilities to complement each other. In experiments, we use a modulation parameter  $\alpha \in (0, 1)$  to balance them as follows:

$$\cos \langle i, j \rangle = \alpha \cos(\mathbf{f}_i^{t'}, \hat{\mathbf{f}}_j') + (1 - \alpha) \cos(\mathbf{f}_i^t, \hat{\mathbf{f}}_j), \quad (10)$$

where  $\cos \langle i, j \rangle$  indicates the integrated similarity between the  $i$ -th detection and the  $j$ -th trajectory at the current time step  $t$ , and will be used for the matching process, as shown in Fig. 2.

## 4. Experiments

### 4.1. Datasets and Metrics

**Datasets.** To evaluate our method, we utilize the following benchmarks. DanceTrack [40] is a challenging multi-dancer tracking dataset featuring diverse movements and highly similar appearances. MOT17 [30] is a classic multiple object tracking dataset, notable for its high density of targets. SportsMOT [7] is a benchmark dedicated to sports events, emphasizing the challenges posed by rapid motion patterns. TAO [8] is a general MOT dataset designed to track nearly all common categories, breaking away from the traditional focus on a single category. These diverse challenges and scenarios presented by these datasets enable a comprehensive validation of both the effectiveness and robustness of our approach.

**Metrics.** On traditional MOT benchmarks [7, 30, 40], we evaluate our method using Higher Order Tracking Accuracy (HOTA) [23], while also including MOTA [2] and IDF1 [36] metrics in some of our experiments. Additionally, to better evaluate the multi-class tracking problem, we employ Tracking Every Thing Accuracy (TETA) [19] on the TAO dataset [8].

Methods	HOTA	DetA	AssA	IDF1
<i>motion-based:</i>				
ByteTrack [49]	47.7	71.0	32.1	53.9
DiffusionTrack [25]	52.4	82.2	33.5	47.5
OC-SORT [5]	55.1	80.3	38.3	54.6
C-BIoU [45]	60.6	81.3	45.4	61.6
<i>hybrid-based:</i>				
FairMOT [48]	39.7	66.7	23.8	40.8
DeepSORT [42]	45.6	71.0	29.7	47.9
StrongSORT [10]	55.6	80.7	38.6	55.2
Deep OC-SORT [27]	61.3	82.2	45.8	61.5
DiffMOT [26]	62.3	82.5	47.2	63.0
<i>reid-based:</i>				
QDTrack [31]	54.2	80.1	36.8	50.4
FastReID-MOT (baseline)	50.6	81.1	31.6	50.4
HAT-FastReID-MOT	58.6	81.3	42.3	57.9
HAT-FastReID-MOT <sup>†</sup>	<b>61.2</b>	<b>81.6</b>	<b>46.0</b>	<b>61.1</b>

Table 1. Performance comparison with state-of-the-art methods on the Dancetrack [40] test set. The best results among feature-based trackers are shown in **bold**.

### 4.2. Implementation Details

**Naïve ReID-Based Tracker.** In modern developments, almost all tracking-by-detection approaches [1, 5, 10, 26, 27, 46, 49] heavily rely on and prioritize position estimation, making it difficult to independently investigate the effects of ReID features. Besides, their tailored designs and multi-stage cascaded matching strategies are also not ideal for clear ablation studies and analysis. Therefore, to seek insightful analysis rather than concentrating on tedious engineering details, we employ a single-stage tracker in this paper that relies solely on ReID features. Specifically, we only use Eq. (2) to calculate feature similarity for constructing the cost matrix and apply the Exponential Moving Average (EMA) to update the trajectory features dynamically. For this baseline tracker, we conduct a grid search on the threshold parameters to find the best configuration, keeping them unchanged in the following experiments. This guarantees the experiments are completely fair and ensures the observed improvements are not from the engineering tweaks. More details are discussed in Appendix A.1.

**Pretrained Models.** To avoid additional training, we apply pre-trained weights from the community for inference throughout this paper. For detector  $\mathcal{D}$ , we generate detection results on traditional datasets [7, 30, 40] using the YOLOX weights provided in the official repositories [5, 7, 49], while for TAO [8], we rely on the detections from MASA [20]. This ensures a fair comparison with contemporary works. By default, we utilize the pre-trained Fas-

Methods	HOTA	DetA	AssA	IDF1
<i>motion-based:</i>				
ByteTrack [49]	63.1	64.5	62.0	77.3
OC-SORT [5]	63.2	63.2	63.4	77.5
C-BIoU [45]	64.1	64.8	63.7	79.7
<i>hybrid-based:</i>				
FairMOT [48]	59.3	60.9	58.0	72.3
DeepSORT [42]	61.2	63.1	59.7	74.5
MixSort-OC [7]	63.4	63.8	63.2	77.8
StrongSORT [10]	64.4	64.6	64.4	79.5
DiffMOT [26]	64.5	64.7	64.6	79.3
<i>reid-based:</i>				
QDTrack [31]	53.9	55.6	52.7	66.3
ContrasTR [32]	58.9	–	–	71.8
FastReID-MOT (baseline)	61.5	63.4	60.0	73.5
HAT-FastReID-MOT†	<b>63.5</b>	<b>64.0</b>	<b>63.2</b>	<b>77.5</b>

Table 2. Performance comparison with state-of-the-art methods on MOT17 [30]. The best results among feature-based trackers are shown in **bold**.

tReID [24] weights from [26, 46] for producing ReID features. For zero-shot MOT research, we adopt MASA [20] as the ReID model, leveraging its outstanding zero-shot transfer performance achieved through training solely on a large-scale image segmentation dataset [18].

### 4.3. State-of-the-art Comparison

In this section, we compare our method with state-of-the-art approaches on several benchmarks [7, 30, 40]. We name the naïve reid-based tracker described in Sec. 4.2 as FastReID-MOT, and the tracker equipped with the proposed **H**istory-**A**ware **T**ransformation as HAT-FastReID-MOT. Similar to mainstream tracking-by-detection methods [5, 26, 27], we also adjust some hyperparameters across various datasets to achieve better tracking results, which are marked with †.

**DanceTrack.** As shown in Tab. 1, due to the extremely similar appearances in group dancing [40], feature-based trackers struggle to achieve satisfactory performance directly. Most methods [5, 10, 27, 46] focus on motion estimation by introducing additional rules to handle nonlinear motion, rather than exploring more discriminative ReID features. However, using the method proposed in this paper, the naïve feature-based tracker can be significantly boosted to achieve comparable performance to the state-of-the-art methods. This demonstrates that our approach effectively enhances the differentiation of highly similar trajectories.

**MOT17.** Since nearly all targets maintain linear movement, utilizing motion estimation for tracking in MOT17 [30] is both efficient and well-suited, as shown in Tab. 2, making additional ReID features often unnecessary [5, 40]. Nev-

Methods	HOTA	DetA	AssA	IDF1
<i>motion-based:</i>				
ByteTrack [49]	62.8	77.1	51.2	69.8
OC-SORT [5]	71.9	86.4	59.8	72.2
ByteTrack [49]	64.1	78.5	52.3	71.4
OC-SORT [5]	73.7	88.5	61.5	74.0
<i>hybrid-based:</i>				
FairMOT [48]	49.3	70.2	34.7	53.5
BoT-SORT [1]	68.7	84.4	55.9	70.0
DiffMOT [26]	72.1	86.0	60.5	72.8
MixSort-Byte [7]	65.7	78.8	54.8	74.1
MixSort-OC [7]	74.1	88.5	62.0	74.4
DiffMOT [26]	76.2	89.3	65.1	76.1
<i>reid-based:</i>				
QDTrack [31]	60.4	77.5	47.2	62.3
FastReID-MOT (baseline)	67.3	86.8	52.3	69.3
HAT-FastReID-MOT	78.1	87.3	69.9	82.4
HAT-FastReID-MOT†	<b>79.3</b>	<b>87.4</b>	<b>72.1</b>	<b>83.6</b>
HAT-FastReID-MOT†	80.8	89.4	73.1	84.7

Table 3. Performance comparison with state-of-the-art methods on SportsMOT [7]. The best results among feature-based trackers are shown in **bold**. Gray results denote joint training involving the validation set of SportsMOT.

ertheless, our method still achieves competitive tracking performance with only appearance features, even surpassing some trackers that leverage hybrid information [7, 42]. This strongly highlights the generalization capability of our method in challenging scenarios.

**SportsMOT.** In Tab. 3, we compare our method on SportsMOT [7] with the latest state-of-the-art methods. Surprisingly, without bells and whistles, our TransFastReID-MOT outperforms all other methods by a large margin, whether motion-based or hybrid-based. Compared to DiffMOT [26], using exactly the same ReID model [24], we achieve a significant advantage (7.2 HOTA). This finding highlights both the obvious potential of appearance features and the need to prioritize them over motion estimation in some situations rather than adhering to a rigid pipeline.

### 4.4. Zero-Shot Comparison

Since our method relies solely on historical trajectories without requiring additional training, we investigate its capability for zero-shot MOT in Tab. 4. These models are sourced from [20], trained solely on a large-scale image segmentation dataset [18], and then zero-shot transferred to the target dataset. Experimental results show that our method consistently leads to significant improvements across various visual encoders [15, 18], showcasing its generalization capability to ReID features from different sources.

Methods	DanceTrack [40] test			SportsMOT [7] test			TAO [8] val	
	HOTA	AssA	IDF1	HOTA	AssA	IDF1	TETA	AssocA
MASA-R50 [20]	50.8	31.6	48.8	71.6	58.9	71.7	45.8	42.7
MASA-Detic [20]	50.6	31.5	50.6	72.2	60.1	73.7	46.5	44.5
MASA-G-DINO [20]	50.4	31.2	49.7	72.8	61.0	74.3	46.8	45.0
MASA-SAM-B [20]	49.4	29.9	48.0	71.9	59.5	72.6	46.2	43.7
HAT-MASA-R50	54.3 (+3.5)	36.1 (+4.5)	54.1 (+5.3)	73.7 (+2.1)	62.4 (+3.5)	75.0 (+3.3)	46.4 (+0.6)	44.4 (+1.7)
HAT-MASA-Detic	54.3 (+3.7)	36.2 (+5.7)	55.3 (+4.7)	74.5 (+2.3)	63.7 (+3.6)	76.7 (+3.0)	47.2 (+0.7)	46.4 (+1.9)
HAT-MASA-G-DINO	53.9 (+3.5)	35.7 (+4.5)	54.5 (+4.8)	74.7 (+1.9)	64.1 (+3.1)	77.1 (+2.8)	47.5 (+0.7)	46.7 (+1.7)
HAT-MASA-SAM-B	52.1 (+2.7)	33.4 (+3.5)	51.9 (+3.9)	73.4 (+1.5)	61.9 (+2.4)	74.8 (+2.2)	46.9 (+0.7)	45.6 (+1.9)

Table 4. Zero-shot transfer multiple object tracking comparisons. All models are trained on a large-scale image segmentation dataset [18] by [20], then zero-shot transferred to these target MOT benchmarks.

#	Detection	Method	$D'$	DanceTrack [40] val				SportsMOT [7] val			
				HOTA	DetA	AssA	IDF1	HOTA	DetA	AssA	IDF1
# 1	Oracle	–	$D$	74.9	97.9	57.3	72.0	86.2	99.4	74.7	84.0
# 2		PCA	$N_{obj} - 1$	75.1	<b>98.0</b>	57.6	72.2	85.6	99.5	73.9	83.6
# 3		PCA	$N_{id} - 1$	56.3	97.5	32.5	50.4	69.4	98.4	49.0	66.4
# 4		FLD	$N_{id} - 1$	<b>79.0</b>	<b>98.0</b>	<b>63.8</b>	<b>77.0</b>	<b>92.2</b>	<b>99.6</b>	<b>85.4</b>	<b>90.7</b>
# 5	YOLOX	–	$D$	51.1	<b>78.3</b>	33.4	51.0	73.7	88.4	61.5	76.6
# 6		PCA	$N_{obj} - 1$	45.3	76.8	26.7	40.0	70.6	88.4	56.4	71.5
# 7		PCA	$N_{id} - 1$	43.5	77.4	24.6	39.4	61.3	88.0	42.7	61.4
# 8		FLD	$N_{id} - 1$	<b>57.7</b>	78.2	<b>42.7</b>	<b>56.7</b>	<b>81.1</b>	<b>88.8</b>	<b>74.1</b>	<b>85.5</b>

Table 5. Comparison of different subspace selections. *Oracle* and *YOLOX* denote the sources of the detection results, while  $D$  and  $D'$  indicate the original and projected feature dimension, respectively.  $N_{obj}$  and  $N_{id}$  represent the total number of historical samples and the number of trajectories. If  $D' > D$ , the target dimension will be set to  $D$ .

Furthermore, we find that our method shows less noticeable improvements on TAO [8] compared to traditional MOT benchmarks [7, 40]. This is likely because the diverse categories of targets in general scenarios make them well-distinguishable in the original space due to lower similarity. Despite this, our approach still achieves improvements. Overall, this not only demonstrates the versatility of our method but also shows its critical role in adapting models to challenging scenarios, which will greatly contribute to the advancement and application of general and open-vocabulary MOT trackers.

#### 4.5. Ablation Study

In this section, we focus on exploring the history-aware transformation of ReID features and evaluating the effectiveness of each module. We use FastReID [24] as our feature extractor and primarily evaluate on DanceTrack [40] due to its known challenge of similar appearance.

**ReID Feature Projection.** As we elaborated in Sec. 3.2, our dissatisfaction with the original space leads us to explore a more effective representation space. In this pa-

per, we opt to use historical features as conditions and employ Fisher Linear Discriminant (FLD) to conduct a linear projection. Likewise, as Principal Component Analysis (PCA) is also a standard method for reducing dimensionality and enhancing the discriminability between samples, we have used PCA in our comparisons. As shown in Tab. 5, using either Oracle or YOLOX detections, projecting the features via Fisher Linear Discriminant (FLD) yields significant performance improvements across different benchmarks [7, 40]. Conversely, using Principal Component Analysis (PCA) not only fails to provide obvious benefits but even introduces adverse effects. We believe this is because PCA does not consider the differences between trajectories in its optimization objective and only aims to separate all samples evenly. This observation reminds us that historical trajectories represent an invaluable asset for MOT. They should be incorporated into reasoning rather than disregarded. We also visualize the ReID features in different spaces in Fig. 3, further validating our perspective.

**History Length  $T$ .** As stated in Sec. 3.3, we maintain a queue of length  $T$  for each trajectory to store the samples

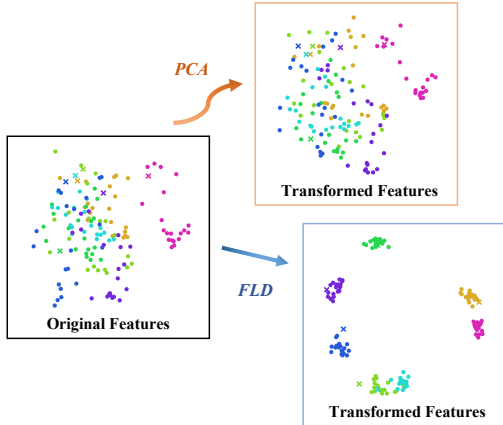


Figure 3. **Visualization ReID features** in the original space and transformed space.  $\bullet$  represents the historical features and  $\times$  indicates the current features. Compared to the other two spaces, the FLD-projected space shows better differentiation of trajectories.

$T$	HOTA	DetA	AssA	MOTA	IDF1
10	54.3	78.3	37.8	<b>86.7</b>	53.2
20	56.2	78.6	40.4	86.5	55.2
40	57.0	<b>78.7</b>	41.4	86.5	56.6
60	<b>57.7</b>	78.2	<b>42.7</b>	86.3	<b>56.7</b>
80	56.3	78.4	40.5	86.2	55.4
$\infty$	55.3	78.4	39.2	85.1	52.2

Table 6. Exploration of the length  $T$  of the historical queue  $\mathcal{F}_j$ . The gray background is the choice as our default setup.

$\lambda_0$	HOTA	DetA	AssA	MOTA	IDF1
1.00	57.7	78.2	42.7	86.3	56.7
0.95	58.5	<b>78.8</b>	42.5	86.8	58.2
0.90	<b>59.3</b>	78.7	<b>44.8</b>	86.9	<b>59.8</b>
0.80	59.1	78.4	44.7	<b>87.0</b>	59.6
0.60	58.1	78.3	43.2	<b>87.0</b>	57.9
0.40	57.8	78.4	42.8	86.9	57.1

Table 7. Investigation of the coefficient  $\lambda_0$  of the temporal-shifted trajectory centroid in Eq. (9). The gray background is the choice as our default setup.

used by Fisher Linear Discriminant (FLD). As the results in Tab. 6, although using a too-short temporal length  $T$  decreases the credibility of the reference samples, it still provides a notable enhancement compared to the baseline tracker without FLD (54.3 vs. 51.1 HOTA). In contrast, an excessively long history queue would make the sample distribution obsolete and lead to negative consequences.

**Temporal-Shifted Trajectory Centroid.** As discussed in

$\alpha$	HOTA	DetA	AssA	MOTA	IDF1
1.0	59.3	<b>78.7</b>	44.8	86.9	59.8
0.9	<b>60.6</b>	78.6	<b>46.8</b>	87.1	<b>61.7</b>
0.8	59.3	78.5	45.0	87.2	60.4
0.6	59.1	78.5	44.7	<b>87.6</b>	60.6

Table 8. Ablations of the coefficient  $\alpha$  of the knowledge integration. The gray background is the choice as our default setup.

Sec. 3.3 and shown in Tab. 6, the importance of samples varies over time in the online tracking process. We propose applying Eq. (9) to shift trajectory centroids, prioritizing recent samples, aiming to discover a projection matrix that aligns more effectively with the current frame. In Tab. 7, we examine different  $\lambda_0$  to regulate the extent of temporal shifting. Experimental results demonstrate that using temporal-shifted trajectory centroid can significantly enhance tracking performance. However, it is important to note that excessively small values of  $\lambda_0$  may lead to an overreliance on recent samples, resulting in a decline in robustness.

**Knowledge Integration.** In Tab. 8, we investigate various fusion coefficients  $\alpha$  to balance robustness and specialization. These results indicate that this is a trade-off art, prompting us to choose 0.9 as our default setting. In addition, this supports the concept outlined in Sec. 3.4, valuing the complementarity of those two spaces can boost the reliability of ReID features.

## 5. Conclusion

In this paper, we revisited the use of ReID features in multiple object tracking (MOT). We pointed out that in most existing studies, the application of appearance features overlooks the specific requirements and characteristics of MOT, reducing it to a generic form of regular ReID tasks, thereby limiting its potential. Therefore, we proposed leveraging historical features as conditions and applying a modified Fisher Linear Discriminant to discover a more discriminative feature space to distinguish different trajectories, fully exploiting the contextual information inherent in MOT. In experiments, we constructed a straightforward feature-based tracker, utilizing only ReID features as tracking cues and excluding elaborate techniques like multi-stage matching. Despite this, the results reveal that our approach matches and even surpasses state-of-the-art tracking performance. This clearly demonstrates the effectiveness of our method and sheds light on the substantial unexploited potential of appearance features. We hope this work could bring ReID features back into the spotlight, encouraging future research to focus on feature extraction and application methods that are better customized and suited for multiple object tracking.

## A. Experimental Details

Some experimental details have to be omitted from the main text due to limited space, but we provide a comprehensive explanation in this section.

### A.1. Naïve ReID-Based Tracker

Although some existing state-of-the-art methods [1, 27, 42, 46] incorporate ReID features as their tracking cues, they usually emphasize and prioritize the position information. For example, Deep OC-SORT [27] integrates appearance features into the first-stage matching based on OC-SORT [5]. Moreover, many approaches [27, 42, 46] employ intricate hyperparameters to carefully balance appearance similarity and positional similarity, along with additional techniques [26, 27] to modulate the cost matrix. We argue that such highly engineered testbeds pose risks that lead us into unintended pitfalls.

Therefore, to ensure clarity in comparisons, as discussed in Sec. (4.2), we employ a simple MOT tracker that relies solely on ReID features. Accordingly, we calculate the cosine similarity between trajectories and detections by Eq. (2). In the experiments, we normalized it to serve as the similarity matrix:

$$\text{similarity}(i, j) = \frac{\cos(\mathbf{f}_i^t, \hat{\mathbf{f}}_j) + 1}{2}, \quad (11)$$

where  $\text{similarity}(i, j)$  indicates the similarity between the  $i$ -th detection and the  $j$ -th trajectory. After that, we calculate the cost matrix as follows:

$$\text{cost}(i, j) = -\text{similarity}(i, j). \quad (12)$$

Finally, the cost matrix is fed into the Hungarian algorithm to obtain the optimal assignment results. Since our tracker is a single-stage design rather than a more complex cascade structure, only three thresholds are used to control this process. First, only the detections with a confidence score greater than  $\tau_{det}$  are considered by our tracker. Second, only assignment pairs with a similarity score above  $\tau_{sim}$  are accepted. At last, any unmatched targets with a confidence score exceeding  $\tau_{new}$  are marked as newborns.

For the trajectory features, we employ the commonly used Exponential Moving Average (EMA) [26, 27, 46] for updating, as shown below:

$$\hat{\mathbf{f}}_j^t = (1 - \alpha_{EMA}) \times \hat{\mathbf{f}}_j^{t-1} + \alpha_{EMA} \times \mathbf{f}_j^t, \quad (13)$$

where  $\alpha$  is a hyperparameter used to control the update ratio. For simplicity, we denote  $\hat{\mathbf{f}}_j^t$  as  $\hat{\mathbf{f}}_j$  throughout this paper. Additionally, during online tracking, a trajectory will be removed if it disappears for more than  $\tau_{miss}$ .

All the aforementioned hyperparameters are tuned using a grid search on the corresponding datasets to obtain optimal settings. In subsequent experiments, we do not adjust these hyperparameters to ensure that the observed improvements are purely attributable to our proposed method.

### A.2. Ablation Details

In the ablation studies presented in Sec. 4.5, we determine each hyperparameter step by step, following the order shown in the table, as marked in `gray` background. Together, these settings make up our default configuration (referenced in Sec 4.3) and are applied uniformly to all datasets ( $T = 60, \lambda_0 = 0.9, \alpha = 0.9$ ).

### A.3. MASA Details

In the MASA [20] inference process, we simplified the original bi-softmax matching procedure [20, 31] to cosine similarity combined with the Hungarian algorithm (as we did in Appendix A.1), which resulted in a slight improvement in tracking performance across all datasets. For our hyperparameters, we primarily adhered to the default settings outlined in Appendix A.2, with the exception of adjusting  $\alpha$  to 0.5 to better accommodate MASA’s feature representation. All hyperparameters remain consistent across different MASA models.

## B. More Results

### B.1. Inference Speed

Given the detection results, our method achieves an inference speed of 22.7 FPS on DanceTrack [40] using an NVIDIA RTX A5000 GPU and an AMD Ryzen 9 5900X CPU. Although this meets the requirements for near real-time tracking, we must point out two main challenges that remain for achieving faster inference.

Based on our experiments, nearly all of the additional latency originates from the computation of eigenvalues and eigenvectors, as this operation is on the CPU (with `scipy.linalg.eigh(S_B, S_W)`), which is inherently inefficient for matrix calculations. We explored some alternative GPU-based packages like PyTorch, JAX, and CuPy. These packages offer CUDA acceleration for eigenvector computations (`eigh()` function). However, they lack an interface for generalized eigenvalue solving in `eigh()` (e.g., discussed in #5461 issue in the official repository of JAX, it only accepts one matrix for the eigenvalue calculation), which is a feature provided by SciPy and used for FLD solution. Transforming the input into a format acceptable for these functions incurs additional computational overhead and results in a loss of precision. If the same interface can be used, we estimate, based on experience, that it would result in a  $4 \times$  to  $10 \times$  speedup.

Moreover, the redundancy in feature dimensions further

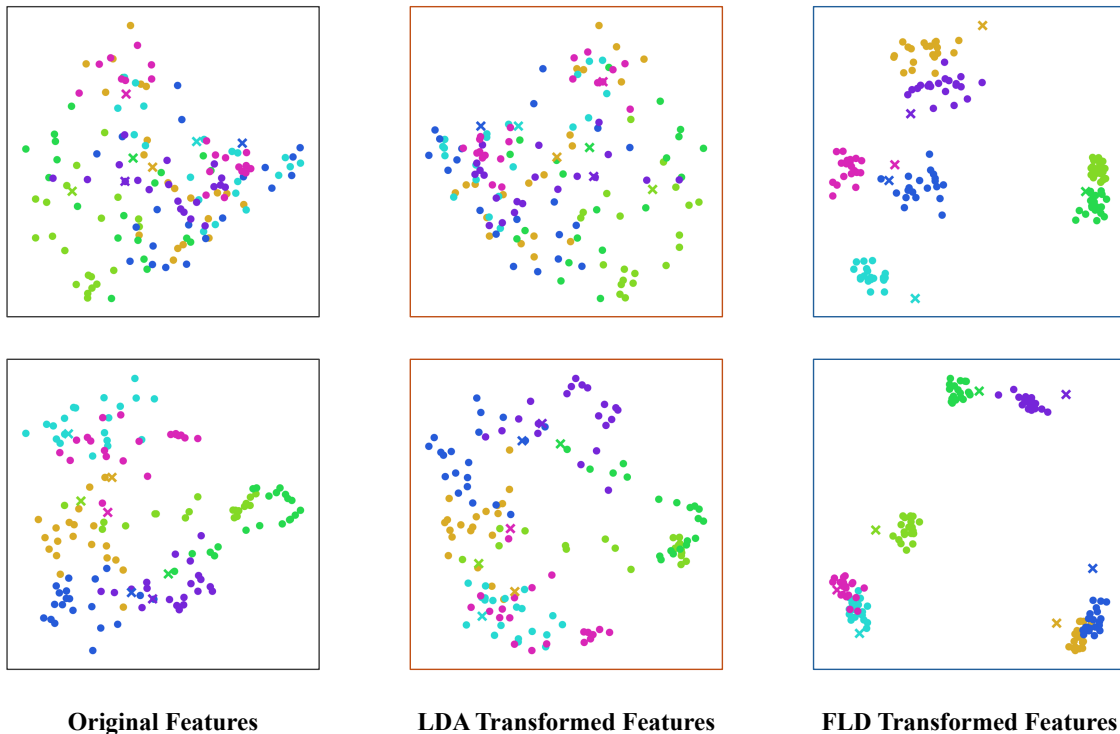


Figure 4. **More visualization of ReID features.** • represents the historical features and ✕ indicates the current features. Compared to the other two spaces, the FLD-projected space shows better differentiation of trajectories.

exacerbates this issue (2048 from FastReID [24] vs. 256 from MASA [20]). In summary, we consider that addressing this operator issue falls beyond the scope of this paper as it pertains to a complicated engineering problem.

## B.2. Visualization

Similar to Fig. 3, we additionally visualized the ReID features of two sequences in different projection spaces. The results indicate that features transformed using FLD exhibit greater differentiation between different trajectories, which facilitates multiple object tracking. As linear dimensionality reduction methods, PCA and FLD are compared to underscore the value of introducing historical assignment information for space selection.

## C. Limitations

Although our approach has yielded encouraging results across various MOT benchmarks, it still leaves some limitations, which warrant further investigation in future work.

Firstly, our tracker design did not incorporate position information. While it performs well overall, we must emphasize that position cues are crucial in some specific scenarios. Therefore, a potential development avenue would

be integrating position information with our method. However, since we have improved the reliability of ReID features, it may be worth reconsidering the current hybrid-based tracker design philosophy, shifting away from prioritizing position information (as discussed in Appendix A.1).

Secondly, in this paper, we only employed a training-free module. We believe that in the future, it may be possible to develop similar learnable methods to enhance the ability to distinguish between different trajectories. This would contribute to improving the generalization and flexibility of the model. Furthermore, we aim to encourage a renewed emphasis and reconsideration of appearance features rather than constraining the enhancement of ReID features solely to this approach. We believe it is crucial to recognize the differing requirements for target features between MOT tasks and ReID tasks, which encourages designing more suitable feature extraction and application methods tailored for MOT rather than blindly adhering to existing practices.

## References

- [1] Nir Aharon, Roy Orfaig, and Ben-Zion Bobrovsky. Bot-sort: Robust associations multi-pedestrian tracking. *CoRR*, abs/2206.14651, 2022. 1, 3, 5, 6, 9
- [2] Keni Bernardin and Rainer Stiefelhagen. Evaluating multi-

- ple object tracking performance: The CLEAR MOT metrics. *EURASIP J. Image Video Process.*, 2008, 2008. 5
- [3] Alex Bewley, ZongYuan Ge, Lionel Ott, Fabio Tozeto Ramos, and Ben Upcroft. Simple online and realtime tracking. In *ICIP*, pages 3464–3468. IEEE, 2016. 1, 2
- [4] Jiarui Cai, Mingze Xu, Wei Li, Yuanjun Xiong, Wei Xia, Zhuowen Tu, and Stefano Soatto. Memot: Multi-object tracking with memory. In *CVPR*, pages 8080–8090. IEEE, 2022. 3
- [5] Jinkun Cao, Xinshuo Weng, Rawal Khirodkar, Jiangmiao Pang, and Kris Kitani. Observation-centric SORT: rethinking SORT for robust multi-object tracking. *CoRR*, abs/2203.14360, 2022. 2, 5, 6, 9
- [6] Nicolas Carion, Francisco Massa, Gabriel Synnaeve, Nicolas Usunier, Alexander Kirillov, and Sergey Zagoruyko. End-to-end object detection with transformers. In *ECCV (1)*, pages 213–229. Springer, 2020. 3
- [7] Yutao Cui, Chenkai Zeng, Xiaoyu Zhao, Yichun Yang, Gangshan Wu, and Limin Wang. SportsMOT: A large multi-object tracking dataset in multiple sports scenes. In *ICCV*, 2023. 5, 6, 7
- [8] Achal Dave, Tarasha Khurana, Pavel Tokmakov, Cordelia Schmid, and Deva Ramanan. TAO: A large-scale benchmark for tracking any object. In *ECCV (5)*, pages 436–454. Springer, 2020. 5, 7
- [9] Patrick Dendorfer, Vladimir Yugay, Aljosa Osep, and Laura Leal-Taixé. Quo vadis: Is trajectory forecasting the key towards long-term multi-object tracking? In *NeurIPS*, 2022. 1, 2, 3
- [10] Yunhao Du, Zhicheng Zhao, Yang Song, Yanyun Zhao, Fei Su, Tao Gong, and Hongying Meng. Strongsort: Make deepsort great again. *IEEE Trans. Multim.*, 25:8725–8737, 2023. 2, 5, 6
- [11] Ronald A Fisher. The statistical utilization of multiple measurements. *Annals of eugenics*, 8(4):376–386, 1938. 2, 3, 4
- [12] K Fukunada. Introduction to statistical pattern recognition. *Computer Science and Scientific Computing*, 1990. 4
- [13] Ruopeng Gao and Limin Wang. MeMOTR: Long-term memory-augmented transformer for multi-object tracking. In *Proceedings of the IEEE/CVF International Conference on Computer Vision (ICCV)*, pages 9901–9910, 2023. 3
- [14] Ruopeng Gao, Yijun Zhang, and Limin Wang. Multiple object tracking as ID prediction. *CoRR*, abs/2403.16848, 2024. 3
- [15] Kaiming He, Xiangyu Zhang, Shaoqing Ren, and Jian Sun. Deep residual learning for image recognition. In *CVPR*, pages 770–778. IEEE Computer Society, 2016. 6
- [16] Hsiang-Wei Huang, Cheng-Yen Yang, Wenhao Chai, Zhongyu Jiang, and Jenq-Neng Hwang. Exploring learning-based motion models in multi-object tracking. *CoRR*, abs/2403.10826, 2024. 2
- [17] Tarasha Khurana, Achal Dave, and Deva Ramanan. Detecting invisible people. In *ICCV*, pages 3154–3164. IEEE, 2021. 2
- [18] Alexander Kirillov, Eric Mintun, Nikhila Ravi, Hanzi Mao, Chloé Rolland, Laura Gustafson, Tete Xiao, Spencer Whitehead, Alexander C. Berg, Wan-Yen Lo, Piotr Dollár, and Ross B. Girshick. Segment anything. In *ICCV*, pages 3992–4003. IEEE, 2023. 6, 7
- [19] Siyuan Li, Martin Danelljan, Henghui Ding, Thomas E. Huang, and Fisher Yu. Tracking every thing in the wild. In *ECCV (22)*, pages 498–515. Springer, 2022. 5
- [20] Siyuan Li, Lei Ke, Martin Danelljan, Luigi Piccinelli, Mattia Segù, Luc Van Gool, and Fisher Yu. Matching anything by segmenting anything. In *CVPR*, pages 18963–18973. IEEE, 2024. 5, 6, 7, 9, 10
- [21] Chao Liang, Zhipeng Zhang, Yi Lu, Xue Zhou, Bing Li, Xiyong Ye, and Jianxiao Zou. Rethinking the competition between detection and reid in multi-object tracking. *CoRR*, abs/2010.12138, 2020. 2
- [22] Zelin Liu, Xinggong Wang, Cheng Wang, Wenyu Liu, and Xiang Bai. Sparsetrack: Multi-object tracking by performing scene decomposition based on pseudo-depth. *CoRR*, abs/2306.05238, 2023. 2
- [23] Jonathon Luiten, Aljosa Osep, Patrick Dendorfer, Philip H. S. Torr, Andreas Geiger, Laura Leal-Taixé, and Bastian Leibe. HOTA: A higher order metric for evaluating multi-object tracking. *Int. J. Comput. Vis.*, 129(2):548–578, 2021. 5
- [24] Hao Luo, Youzhi Gu, Xingyu Liao, Shenqi Lai, and Wei Jiang. Bag of tricks and a strong baseline for deep person re-identification. In *CVPR Workshops*, pages 1487–1495. Computer Vision Foundation / IEEE, 2019. 1, 2, 3, 6, 7, 10
- [25] Run Luo, Zikai Song, Lintao Ma, Jinlin Wei, Wei Yang, and Min Yang. Diffusiontrack: Diffusion model for multi-object tracking. In *AAAI*, pages 3991–3999. AAAI Press, 2024. 5
- [26] Weiyi Lv, Yuhang Huang, Ning Zhang, Ruei-Sung Lin, Mei Han, and Dan Zeng. Diffmot: A real-time diffusion-based multiple object tracker with non-linear prediction. In *CVPR*, pages 19321–19330. IEEE, 2024. 2, 3, 5, 6, 9
- [27] Gerard Maggolino, Adnan Ahmad, Jinkun Cao, and Kris Kitani. Deep oc-sort: Multi-pedestrian tracking by adaptive re-identification. *arXiv preprint arXiv:2302.11813*, 2023. 2, 3, 5, 6, 9
- [28] Gianluca Mancusi, Aniello Panariello, Angelo Porrello, Matteo Fabbri, Simone Calderara, and Rita Cucchiara. Trackflow: Multi-object tracking with normalizing flows. In *Proceedings of the IEEE/CVF International Conference on Computer Vision*, pages 9531–9543, 2023. 2
- [29] Tim Meinhardt, Alexander Kirillov, Laura Leal-Taixé, and Christoph Feichtenhofer. Trackformer: Multi-object tracking with transformers. In *CVPR*, pages 8834–8844. IEEE, 2022. 3
- [30] Anton Milan, Laura Leal-Taixé, Ian D. Reid, Stefan Roth, and Konrad Schindler. MOT16: A benchmark for multi-object tracking. *CoRR*, abs/1603.00831, 2016. 5, 6
- [31] Jiangmiao Pang, Linlu Qiu, Xia Li, Haofeng Chen, Qi Li, Trevor Darrell, and Fisher Yu. Quasi-dense similarity learning for multiple object tracking. In *CVPR*, pages 164–173. Computer Vision Foundation / IEEE, 2021. 5, 6, 9
- [32] Pierre-François De Plaen, Nicola Marinello, Marc Proesmans, Tinne Tuytelaars, and Luc Van Gool. Contrastive learning for multi-object tracking with transformers. In *WACV*, pages 6853–6863. IEEE, 2024. 3, 6

- [33] Zheng Qin, Sanping Zhou, Le Wang, Jinghai Duan, Gang Hua, and Wei Tang. Motiontrack: Learning robust short-term and long-term motions for multi-object tracking. In *CVPR*, pages 17939–17948. IEEE, 2023. 2
- [34] C Radhakrishna Rao. The utilization of multiple measurements in problems of biological classification. *Journal of the Royal Statistical Society. Series B (Methodological)*, 10(2): 159–203, 1948. 3
- [35] Ergys Ristani and Carlo Tomasi. Features for multi-target multi-camera tracking and re-identification. In *CVPR*, pages 6036–6046. Computer Vision Foundation / IEEE Computer Society, 2018. 1
- [36] Ergys Ristani, Francesco Solera, Roger S. Zou, Rita Cucchiara, and Carlo Tomasi. Performance measures and a data set for multi-target, multi-camera tracking. In *ECCV Workshops (2)*, pages 17–35, 2016. 5
- [37] Leonardo Saraceni, Ionut Marian Motoi, Daniele Nardi, and Thomas A. Ciarfuglia. Agrisort: A simple online real-time tracking-by-detection framework for robotics in precision agriculture. In *ICRA*, pages 2675–2682. IEEE, 2024. 2
- [38] Mattia Segù, Luigi Piccinelli, Siyuan Li, Yung-Hsu Yang, Bernt Schiele, and Luc Van Gool. Samba: Synchronized set-of-sequences modeling for multiple object tracking. *CoRR*, abs/2410.01806, 2024. 3
- [39] Peize Sun, Yi Jiang, Rufeng Zhang, Enze Xie, Jinkun Cao, Xinting Hu, Tao Kong, Zehuan Yuan, Changhu Wang, and Ping Luo. Transtrack: Multiple-object tracking with transformer. *CoRR*, abs/2012.15460, 2020. 3
- [40] Peize Sun, Jinkun Cao, Yi Jiang, Zehuan Yuan, Song Bai, Kris Kitani, and Ping Luo. Dancetrack: Multi-object tracking in uniform appearance and diverse motion. In *CVPR*, pages 20961–20970. IEEE, 2022. 1, 5, 6, 7, 9
- [41] Zhongdao Wang, Liang Zheng, Yixuan Liu, Yali Li, and Shengjin Wang. Towards real-time multi-object tracking. In *ECCV (11)*, pages 107–122. Springer, 2020. 2
- [42] Nicolai Wojke, Alex Bewley, and Dietrich Paulus. Simple online and realtime tracking with a deep association metric. In *ICIP*, pages 3645–3649. IEEE, 2017. 2, 3, 5, 6, 9
- [43] Changcheng Xiao, Qiong Cao, Zhigang Luo, and Long Lan. Mambatrack: A simple baseline for multiple object tracking with state space model. In *ACM Multimedia*, pages 4082–4091. ACM, 2024. 2
- [44] Feng Yan, Weixin Luo, Yujie Zhong, Yiyang Gan, and Lin Ma. Bridging the gap between end-to-end and non-end-to-end multi-object tracking, 2023. 3
- [45] Fan Yang, Shigeyuki Odashima, Shoichi Masui, and Shan Jiang. Hard to track objects with irregular motions and similar appearances? make it easier by buffering the matching space. In *WACV*, pages 4788–4797. IEEE, 2023. 2, 5, 6
- [46] Mingzhan Yang, Guangxin Han, Bin Yan, Wenhua Zhang, Jinqing Qi, Huchuan Lu, and Dong Wang. Hybrid-sort: Weak cues matter for online multi-object tracking. *CoRR*, abs/2308.00783, 2023. 2, 3, 5, 6, 9
- [47] Fangao Zeng, Bin Dong, Yuang Zhang, Tiancai Wang, Xiangyu Zhang, and Yichen Wei. MOTR: end-to-end multiple-object tracking with transformer. In *ECCV (27)*, pages 659–675. Springer, 2022. 3
- [48] Yifu Zhang, Chunyu Wang, Xinggang Wang, Wenjun Zeng, and Wenyu Liu. Fairmot: On the fairness of detection and re-identification in multiple object tracking. *Int. J. Comput. Vis.*, 129(11):3069–3087, 2021. 2, 5, 6
- [49] Yifu Zhang, Peize Sun, Yi Jiang, Dongdong Yu, Fucheng Weng, Zehuan Yuan, Ping Luo, Wenyu Liu, and Xinggang Wang. Bytetrack: Multi-object tracking by associating every detection box. In *ECCV (22)*, pages 1–21. Springer, 2022. 1, 2, 5, 6
- [50] Yuang Zhang, Tiancai Wang, and Xiangyu Zhang. Motrv2: Bootstrapping end-to-end multi-object tracking by pre-trained object detectors, 2022. 3
- [51] Xingyi Zhou, Vladlen Koltun, and Philipp Krähenbühl. Tracking objects as points. In *ECCV (4)*, pages 474–490. Springer, 2020. 2
- [52] Xingyi Zhou, Tianwei Yin, Vladlen Koltun, and Philipp Krähenbühl. Global tracking transformers. In *CVPR*, pages 8761–8770. IEEE, 2022. 2
- [53] Xizhou Zhu, Weijie Su, Lewei Lu, Bin Li, Xiaogang Wang, and Jifeng Dai. Deformable DETR: deformable transformers for end-to-end object detection. In *ICLR*. OpenReview.net, 2021. 3